Int. J. Electrochem. Sci., 12 **(2017)** 7795 – 7806, doi: 10.20964/2017.08.29

International Journal of ELECTROCHEMICAL SCIENCE
www.electrochemsci.org

Fabrication and Electrochemical Properties of $Li_4Ti_5O_{12}$@Li_6PS_5Cl for All-solid-state Lithium Batteries using Simple Mechanical Method

Ailing Hwang, Yulin Ma, Yi Cao, Qin Li, Long Wang, Xinqun Cheng, Pengjian Zuo, Chunyu Du, Yunzhi Gao[*]*, Geping Yin*

MIIT Key Laboratory of Critical Materials Technology for New Energy Conversion and Storage, School of Chemistry and Chemical Engineering, Harbin Institute of Technology, Harbin 150001, China
[*]E-mail: gao_yunzhihit@hit.edu.cn

Received: 17 April 2017 / *Accepted:* 5 June 2017 / *Published:* 12 July 2017

Li_6PS_5Cl-coated $Li_4Ti_5O_{12}$ materials was fabricated by a simple liquid-phase treatment method. Charge-discharge tests show that Li_6PS_5Cl-coated $Li_4Ti_5O_{12}$ (LTO@LPSCl)/Li_6PS_5Cl/Li all-solid-state lithium batteries exhibit high reversible capacity (~158 mA h·g^{-1}) after 250 cycles under 0.05 C and excellent rate capacity (~50 mA h·g^{-1}) under 1 C at 80 ℃.A combination of scanning electron microscopy (SEM), energy dispersive X-ray analysis (EDX) mapping, and electrochemical impedance spectra (EIS) reveals that good wettability of liquid with $Li_4Ti_5O_{12}$ materials and Li_6PS_5Cl is responsible for Li_6PS_5Cl nanoparticle coated on the surface of $Li_4Ti_5O_{12}$ materials homogenously, which build the stable interface between active materials and solid state electrolyte, reduce the interface resistance effectively, and result in excellent electrochemical performances.

Keywords: all-solid-state lithium battery**,** electrode-electrolyte interface**,** 200#Paint solvent, $Li_4Ti_5O_{12}$@Li_6PS_5Cl nanocomposites**,** liquid-phase method

1. INTRODUCTION

Lithium secondary batteries have been used to power laptops, mobile phones, electric cars, etc. because of their high operating voltage, high energy density, and long cycle performance [1]. However, liquid electrolytes make themselves prone to risks of leakage and ignition, which slash the safety, the primary concern to customers, of lithium ion batteries. Recently, the so called “all-solid-state lithium secondary batteries” (ASSLBs) using inorganic solid electrolytes have been recognized as good alternatives due to their high energy density, excellent safety, efficient packing, and versatility in

battery geometry [2, 3]. Despite these great promises, the commercialization of ASSLBs has still many obstacles to overcome, including interface resistance between electrodes (anode and cathode) and electrolytes, ionic conductivity and windows of bulk-type electrolytes, cyclic stability, rate performance, etc.

In fact, solid electrolytes have lower ionic conductivities compared with liquid electrolytes and this property is very important to the electrochemical performance of batteries. For ASSLBs, solid electrolytes require an ionic conductivity of at least 10^{-3} $S \cdot cm^{-1}$ for practical application [4]. Many researches have focus on the bulk-type electrolytes to improve the ionic conductivity in past years. Among these electrolytes, sulfide-based solid electrolytes show the excellent lithium-ion conductivity [5-7]. The lithium argyrodite, characterized by the original composition Li_7PnCh_6, makes up a great and promising candidate of solid state electrolytes in ASSLBs for its remarkable ion conductivity. Niek [8] et al. predicted an optimal Cl distribution of 1:3 over sites 4a and 4c for Li_6PS_5Cl, bringing about a Li-ion conductivity twice as high as that of the conventional solid materials. Deiseroth [9] et al. synthesized the Li-argyrodite crystals with formula Li_6PS_5X (X = Cl, Br, I) and Li_7PS_6. The Li-ion conductivity of Li_6PS_5Cl was up to 10^{-3} $S \cdot cm^{-1}$ at room temperature, approximating that of typical liquid electrolytes and this kind of solid electrolyte showed its excellent electrochemical performance [10-12]. Thus, it can be served as a potential electrolyte for ASSLBs.

However, Li_6PS_5Cl electrolyte still suffers confused interfacial phenomena, such as undesired interfacial side reaction between electrodes and electrolyte, lattice deformation of Co element etc. Especially, the space-charge layer (SCL) [3, 13-15] caused by the interfacial Li-ion depletion makes lithium ions difficultly strive across the interface between oxide cathodes and Li_6PS_5Cl electrolyte. This possible mechanism is supported by disappearance of the potential slope with increasing thickness of the buffer layers at initial charging process. What's more, Ohta and co-workers improved the interfacial Li-ion conductivities by covering the surface of the $LiCoO_2$ (LCO) particles with buffer layers of $Li_4Ti_5O_{12}$ (LTO) [16], $LiNbO_3$ (LNO) [17], $LiTaO_3$ [13], and Li_2SiO_3 [18]. Haruyama [19] reported their investigation of interfaces between the LCO/Li_7PS_6 and the LCO/LNO/Li_7PS_6. They found that the intervention of the $LiNbO_3$ layers brought in smoothly uniform interfaces and suppressed the formation of space-charge layer and Li ions' inhomogeneously distribution.

Various interfaces between the electrodes and electrolytes distinguish ASSLBs from conventional ones using liquid electrolytes composed of $LiPF_6$ salt dissolved in carbonates. Since both electrode and electrolyte materials are solid, and electrochemical reactions occur through the solid-solid interface, the interface's structure and morphology play important roles in a battery's electrochemical performance. Hence, the design of composite electrodes turns out to be particularly important to secure densely packed interfaces and solid-solid contact with highly conducting network and paths of lithium ions. Recently, many studies have been carried out to construct an ideal electrode-electrolyte interface in ASSLBs [13, 16-18, 20-23]. Sakuda reported that coating $LiCoO_2$ with $Li_2SeP_2S_5$ or Li_4GeS_4-Li_3PS_4 solid electrolyte by the pulsed laser deposition (PLD) was an effective approach to form a favorable electrode-electrolyte interface [16, 20, 21]. Hirokazu reported an attempt to prepare composite electrode with Li_2S–P_2S_5 glasses as active materials [24]. Shingo Teragawa tried to use ethanol to conduct a favorable interface between $LiCoO_2$ electrode and sulfide-based electrolyte [25-27]. However, these methods suffer from large-scale equipment such as PLD or fluidized bed

reactor and corresponding complex synthesis operation which cost vast time and a large amount of investment, not to mention some of those undesirable electrochemical performances.

As we all know, the composite electrode should contain active materials and conductive agents as well as solid electrolyte at the same time. The favorable interfaces can be easily prepared by using the liquid-phase method which is a much simpler and cheaper process than other methods. However, the hydrophobous electrode compared with conventional electrolytes makes it an obstacle to achieve the physical contact environment so that we can disperse all these all-solid-state powders. Despite various prepared composite electrodes using only dry mixing methods with an agate mortar[28, 29], their unsatisfied electrochemical properties are not suitable for further applications. In addition, the nanoparticles are capable agglomerated through the mixture, for instance the Super P which is widely used as conductive agent. Hence, for the uniformly mixture and performance enhancement of the composite electrode, it is crucial to figure out certain liquid-phase method.

Seeking suitable materials to match with solid electrolyte is another advisable method to ameliorate electrode-electrolyte interface. The representative material $Li_4Ti_5O_{12}$, as identified by Ohzuku et al. [30], has a good reversibility and the negligible volume change in the charge-discharge process, which are the ideal characteristics for the stability of electrode/electrolyte interface in ASSLBs. Hence, $Li_4Ti_5O_{12}$ can be demonstrated as a promising option for all-solid-state lithium ion batteries, without the risks of emergence of flammable gas mixtures and electrolyte decomposition occurr in conventional batteries when large amounts of liquid electrolyte are used.

Here, we successfully prepared anhydrous LPSCl electrolyte and LTO@LPSCl composite to construct $Li_4Ti_5O_{12}$ (LTO)/ Li_6PS_5Cl (LPSCl) /Li ASSLBs with favorable electrode/electrolyte interface and optimized electrochemical performance. Coating of the solid electrolytes on $Li_4Ti_5O_{12}$ particles was carried out by liquid-phase method using brand-new solvent, 200#Paint, so that the uniform interface between electrode and solid electrolyte with a large contact area was formed. The 200#Paint proposed by us firstly has many advantages as a solvent, for instance, a lower distil-off temperature which should be effective in preventing side-reactions between the electrolyte coating layer and electrode particles during heat-treatment for removing the solvent. What's more, this 200#Paint is cheaper and hypotoxic compared with other solvents such as the N-methlyformamide solvent.

The ASSLBs were fabricated by cold-press method and further characterized in coin-cells. From the perspective of recent research status, the cell exhibited superior rate capacity and excellent cycling stability. Additionally, we compared the electrochemical properties of the cell using electrolyte-coated $Li_4Ti_5O_{12}$ with non-coated $Li_4Ti_5O_{12}$ to clarify the performance optimization owing to the coating effect. As described in this paper, we demonstrated the electrochemical performance at a high temperature of 80 ℃. It is difficult for liquid-electrolyte batteries to operate at a temperature of 80 ℃ because of thermal runaway. Nevertheless, charge-discharge analysis at that temperature is propitious to describe features of all-solid-state batteries.

As described above, it is readily apparent that this easy but efficient method for forming conformal interfaces between electrode and sulfide solid electrolyte is beneficial to extensive application of ASSLBs.

2. EXPERIMENTAL

2.1 Preparation of electrolytes and fabrication of all-solid-state cells

Synthesis of solid electrolytes Li_6PS_5Cl (LPSCl) was conducted by solid-phase method. Reagent-grade Li_2S (Hawk 99.9%), P_2S_5 (Aladdin 99%), and LiCl (Aladdin 99%) crystalline powders as starting materials were mixed in stoichiometric proportions. The mechanical milling treatment was conducted using a planetary ball milling apparatus. A rotation speed was fixed at 600 rpm during 10 h via an intermittent step at room temperature. The collected powders after ball-milling were heated in a quartz holder placed in a tubular furnace under vacuum for 5 h at 550 °C. After natural cooling, LPSCl solid electrolyte was obtained. LTO particles, LPSCl and VGCFs (Vapor grown carbon fibres) with the weight ratio of 5:4:1 were dispersed into 200#Paint solvent. After stirring for 24 h at room temperature, the prepared solution was dried at 60 ℃ for 24 h and then LTO@LPSCl/VGCFs composites were obtained. The whole preparing process of the electrode is operated in the glove-box filled with Ar gas, and the detailed process is demonstrated in Fig. 1.

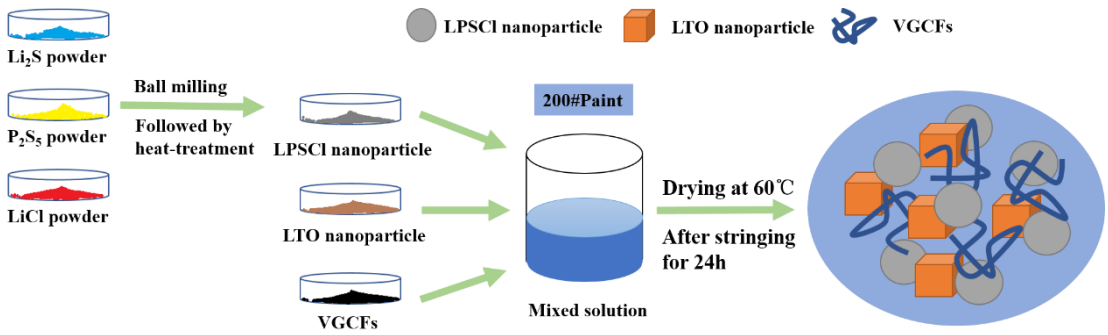

Figure 1. Preparing process of the nanomaterial used in this paper via liquid-phase mixture with 200#Paint solvent.

All-solid-state cells were fabricated as follows. A bilayer pellet (16 mm in diameter) consisting of the LTO@LPSCl/VGCFs composites (about 10mg) as a positive electrode layer and the solid electrolytes Li_6PS_5Cl as a ionic-conducting separator (160 mg) was prepared by co-pressing under 300 MPa, and the lithium metal was attached to the pellet to assemble a CR2025 button cell. All processes were performed under argon atmosphere with the content of H_2O below 0.5 ppm.

2.2 Characterization and Electrochemical measurements

The as-prepared LPSCl samples were characterized by X-ray diffraction (XRD) patterns conducted by a PANaltical Empyrean X-Ray Diffractometer with Cu Kα radiation. The morphologies and energy dispersive X-ray analysis (EDX) elements mapping of LTO@LPSCl composite were observed by a field-emission scanning electron microscope (FEI Helios Nanolab 600i) with an energy dispersive X-ray spectroscopy system. To measure the ionic conductivities of the LPSCl electrolyte,

pelletized samples were prepared by cold pressing method (ϕ15 mm, ~0.50 mm thickness, 330MPa), and electrochemical impedance spectroscopy (EIS) of LPSCl electrolyte with stainless steel/LPSCl/stainless steel structure was performed on the PARSTAT-2273 advanced electrochemical system (Princeton Applied Research) in a frequency range of 100 kHz - 0.01 Hz with amplitude of 5 mV. DC polarization measurement was carried out with Neware battery test systems for the electronic conductivity of the electrolyte. AC-impedance spectrum of LTO@LPSCl/LPSCl/Li cells before cycling was tested under the same frequency range and machine as previously describe.

Electrochemical performances of LTO@LPSCl composites with LPSCl solid electrolytes were evaluated on Neware battery test systems in the voltage range from 1.0 V to 2.5 V (vs. Li^+/Li) at 80 ℃. The galvanostatic charge/discharge cycling test of the LTO@LPSCl/LPSCl/Li cells was operated at a constant current of 0.05 C (1 C = 175 mA g^{-1}). For the rate capability test, the cells were cycled at various rates of 0.05 C, 0.1 C, 0.5 C, 1 C for 5 cycles, respectively, then back to 0.05 C for the last 5 cycles.

3. RESULTS AND DISCUSSION

Fig. 2a shows the XRD patterns for the phase analysis of the as-prepared LPSCl electrolyte. It is obvious that characteristic diffraction peak position indexes well with standard Li_6PS_5Cl reported [31], which indicates that crystallized argyrodite Li_6PS_5Cl phase spontaneously forms after ball-milling and heat-treatment. Moreover, no impurity peaks occur, affirming the formation of pure crystallized Li_6PS_5Cl phase. Ionic conductivity is another important character of the resultant LPSCl electrolyte, which was determined from AC impedance spectrum (Fig. 2b) performed using a stainless steel/LPSCl/Pt stainless steel sandwich structure. A straight line instead of semicircle is observed in the spectrum over the entire frequency range, indicating extremely low grain boundary resistance of the LPSCl electrolyte. The total ionic conductivity (up to 1.6×10^{-3} $S\cdot cm^{-1}$) is simply calculated from the formula ($\delta=L/(R\times S)$), where R is the resistance value corresponding to the intercept of the x-axis. L and S are the thickness and superficial area of the electrolyte pellet, respectively. In addition, the electronic conductivity of the LPSCl electrolyte was further evaluated according to the potentiostatic DC polarization curve (inset in Fig. 2b), which was measured with the same stainless steel/LPSCl/Pt stainless steel structure. By fitting the time dependency of the current with a suitable fit function (exponential decay of second order), a stationary current value is extrapolated at the end of the curve. Consequently, the electronic conductivity is obtained according to Ohm's law, which is up to 3×10^{-8} $S\cdot cm^{-1}$. The high ionic conductivity and negligible electronic conductivity of the as-prepared LPSCl electrolyte are due to the summary of the structural studies and the bond valence models. Prasada concluded that fast ion transport in the argyrodites results from the ion mobility enhanced by the PS_4^{3-} anions and thereby smaller halide ions [32].

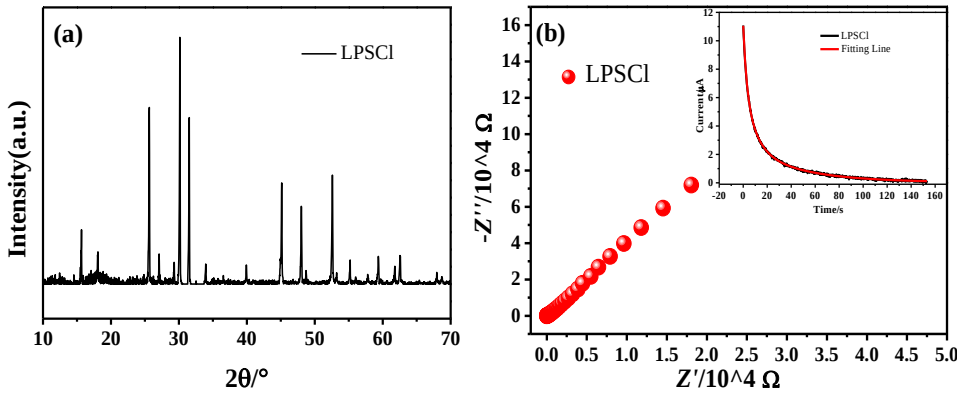

Figure 2. X-ray diffraction(XRD) patterns of the LPSCl (a) and Electrochemical impedance measurements (b) and DC polarization measurements (inset) of the LPSCl electrolyte pressed under 330MPa.

Fig. 3a exhibits XRD patterns for the obtained LTO@LPSCl sample prepared subsequently by simply coating the as-synthesized LPSCl on LTO particles with the assistance of 200#Paint solvent. Evidently, the diffraction peaks of the LTO@LPSCl composite are assigned to original LTO and LPSCl electrolyte. Moreover, no diffraction peaks of impurities are detected, verifying that no side-reactions occur between LTO and LPSCl during the liquid-phase coating process via 200#Paint solution.

The morphology and microstructure of the LTO@LPSCl composite mixed with VGCF were observed by SEM and EDX element mapping (Ti, S and Cl). As shown in Fig. 3b, the primary LTO particles agglomerated and formed micrometer-sized particles during the liquid-phase preparation process, and the mashed solid electrolyte particles evenly dispersed over the surface of LTO particles. A representative particle of LTO (Fig. 3c) and the EDX mapping signals of Ti, S and Cl elements (Fig. 3d-f) further indicated the uniform distribution of LPSCl electrolyte on the surface of LTO particles, suggesting the effective coating via simple liquid-phase method with 200#Paint solvent. In addition, VGCFs are also visible and distributed among LTO@LPSCl agglomerates in Fig. 3b. These long fibers are benefit to construct favorable electronic pathways and connect the LPSCl electrolytes, which will make contributions to high electronic conductivity of the electrodes. The morphology and microstructure prove that liquid phase method with 200#Paint solvent can construct a conformal interface between solid electrode and electrolyte used in this paper.

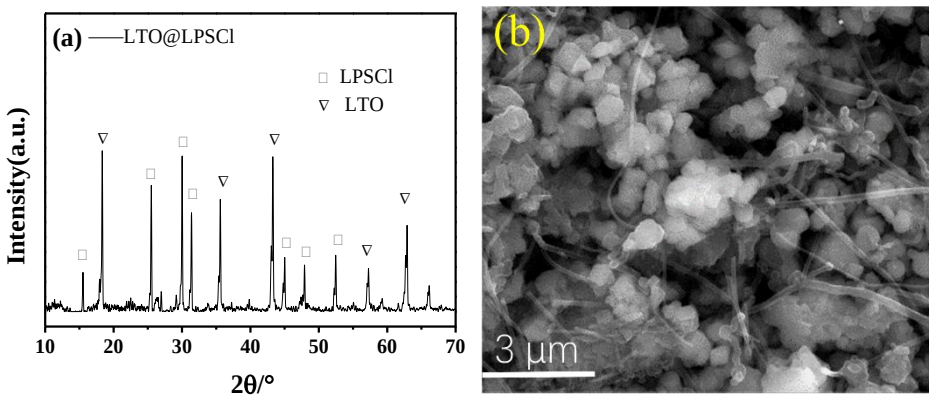

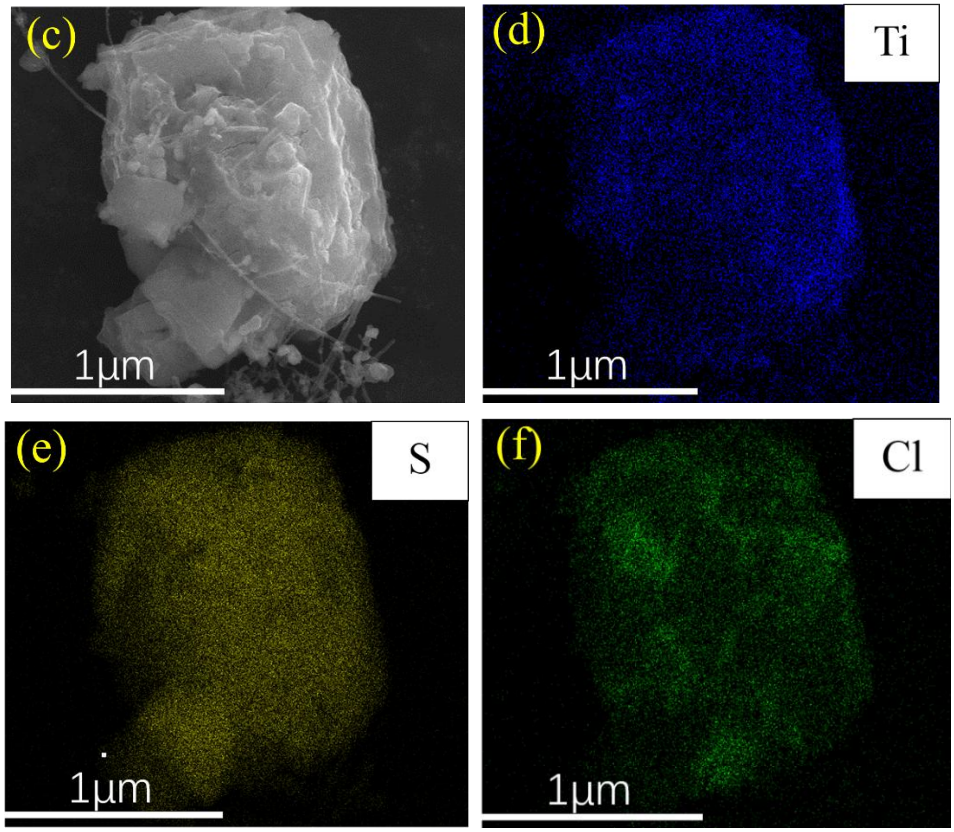

Figure 3. X-ray diffraction(XRD) patterns of the LTO@LPS powders (a) prepared from the 200#Paint solution after drying at 60 ℃ under argon atmosphere and Scanning electron microscopy and energy dispersive X-ray analysis (EDX) mapping (Ti, S and Cl) images of LTO particles coated with the LPSCl electrolyte (b-f).

To evaluate the cyclic performance of LTO@LPSCl/Li cells, galvanostatic charging and discharging measurement at 0.05 C is performed at 80 ℃. Fig. 4a shows the charge/discharge curves of 1st, 2nd, and 100th cycles for LTO@LPSCl/Li cells in the potential range of 1.0-2.5 V. A conspicuous plateau appears in the potential-capacity curves. The charge potential and discharge potential are both near 1.55 V, which indicates a two phase reaction, as the $Li_4Ti_5O_{12}$ converts to $Li_7Ti_5O_{12}$ [33]. The initial specific discharge and charge capacities are 179.6 mA $h \cdot g^{-1}$ and 168.0 mA $h \cdot g^{-1}$, respectively, corresponding to a high initial Coulombic efficiency of 93.5%. The irreversible capacity loss ought to be attributed to the incomplete reduction of Ti^{4+} to Ti^{3+}. Wu's XPS results [34] detected the presence of traces of Ti^{3+} during the first lithiation, suggesting that the reduction of LTO does not reach the 100% reversibility in the progress of delithiation. From the second cycle onward, the charge profiles tend to overlap at subsequent cycles, implying a relatively steady cycle performance of LTO@LPSCl/Li cells.

The cycling performance of the LTO@LPSCl/Li cells under 0.05 C at 80 ℃ is depicted in Fig. 4b. The capacity decreases little during the 250 cycles. The stability of the LTO@LPSCl/Li-based cell suggests no reaction occurring through the interface between the LPSCl electrolyte and lithium foil during cycling. The Li_2S-LiCl-P_2S_5 matrix obtained is like to become a protect layer and demonstrates

the feasibility of employing lithium foil instead of Indium or Li-In alloy as counter electrode [35]. Specifically, the charge capacity of 158.4 mA $h \cdot g^{-1}$ is retained after 250 cycles, corresponding to high capacity retention of about 94.3%. In addition, the Coulombic efficiency is almost above 99% from the 5th onward. This superior cyclability is ascribed to the facilitative ion diffusion between LTO and LPSCl electrolyte and improved utilization of LTO because of the surface coating of LPSCl. From the perspective of recent research status, the cell exhibited superior rate capacity and excellent cycling stability.

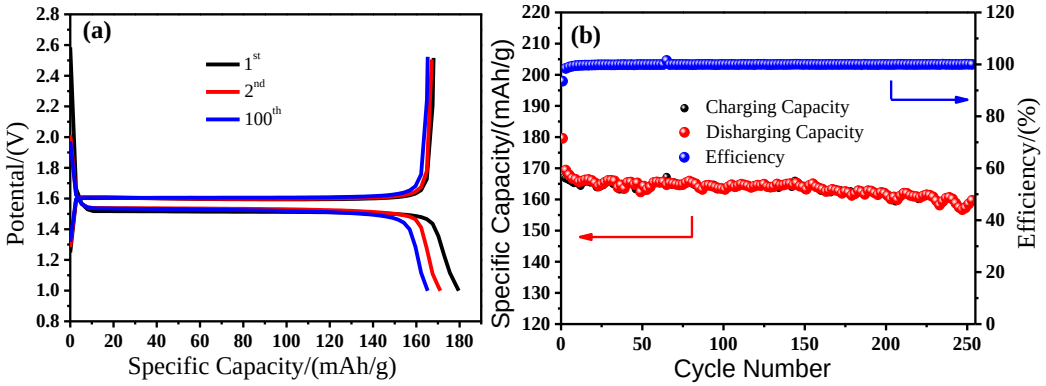

Figure 4. The charge-discharge curves at 0.05 C(a), the long cycling stability (b) at 0.05 C of the cells using LTO@LPSCl nanocomposite electrode and LTO electrode at 80 ℃.

Due to the characteristics such as hydrophobicity and frangibility, only a few of those measurements used in conventional batteries can be imitated for solid–solid interfaces. Electrochemical impedance spectroscopy (EIS), is one of the most important technology to separate the electrochemical processes based on characteristic frequencies or capacitance of each process. In order to figure out the reason of the excellent electrochemical performance, the AC-impedance spectrum of LTO@LPSCl/LPSCl/Li is shown in Fig. 5a. For comparison, the impedance plots of the non-coated LTO/LPSCl/Li all-solid-state cell were also presented in Fig. 5a to further identify the effects of the LPSCl coating on the internal resistance of all-solid-state cells. The resistance in the high frequency region, which possibly contains the resistance derived from the composite electrode, is mainly ascribed to the resistance of the solid electrolyte layer [24]. The barely detected value is in agreement with the resistance measured in previous EIS characterization. Both impedance spectra exhibit a depressed semicircle at medium-low frequency region owing to the electrode-electrolyte interface resistance R_i [36]. Obviously, the value of R_i in LTO@LPSCl/Li cell is much lower than that in non-coated LTO /Li cell, indicating the ameliorative interface performance due to the LPSCl coating with large contact areas via a simple liquid-phase post-treatment in 200#Paint solution.

The capacity of LTO@LPSCl/ LPSCl/Li cells at a series of rates from 0.05 C to 1.0 C were measured at 80 ℃ to further demonstrate the effects of LPSCl coating layer on the electrochemical performance, as shown in Fig. 5b. Clearly, the LTO@LPSCl electrode exhibits a remarkable superior rate capability compared with non-coated LTO counterpart, delivering average capacities of 170.7, 104.4, 73.8, and 47.9 mA $h \cdot g^{-1}$ with the current densities of 0.05, 0.1, 0.5, 1.0 C, respectively.

Moreover, the average capacity restores to 162.2 mA $h \cdot g^{-1}$ while the rate is set back to 0.05 C, indicating its decent rate capability with LPSCl coating. In contrast, the cell fabricated from non-coated LTO electrode does not operate sufficiently, and ultra-low capacity of 7.2 and 3.7 mA $h \cdot g^{-1}$ at 0.5, 1.0 C is observed, respectively. During the charge-discharge process, there is a spontaneous equilibrium exchange of Li-ions between Li-rich and Li-poor phases [37]. Comparison with the results conducted by Yu et al. [38], this interfacial reaction leads to an additional overpotential. Good agreement is established between this overpotential and previous loss of initial capacity. With the increasing current, the overpotential grows and finally becomes the major hurdle for Li-ions transport. These results suggest that the improved rate capability and enhanced capacity of LTO@LPSCl electrode mainly assign to the decreased internal resistance and favorable internal interface due to LPSCl coating in 200# Paint solvent.

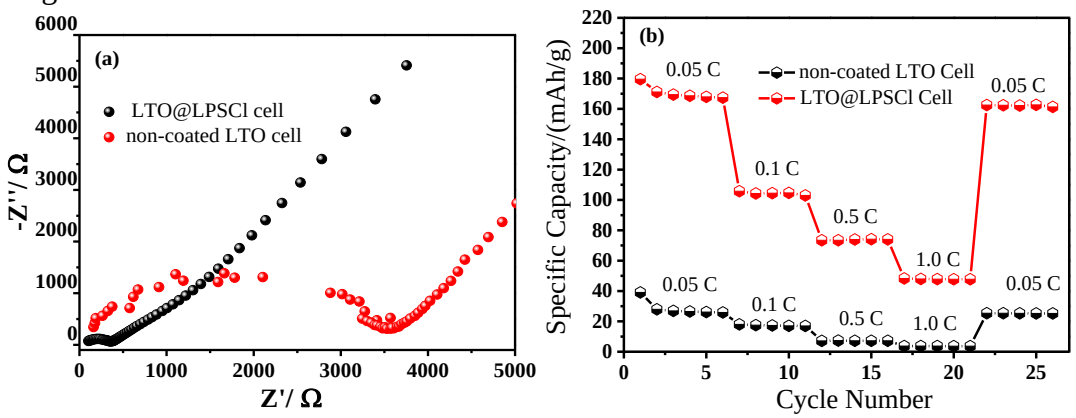

Figure 5. Electrochemical impedance spectra (a) and The rate performance (b) of the cells using electrolyte-coated LTO and non-coated LTO under 0.05 C-1 C.

Based on the above experimental results and discussions combined with published reports, a direct-viewing schematic is presented in Fig. 6 to illustrate the reasons for the enhanced electrochemical performance of LTO@LPSCl electrode derived from liquid-phase post-treatment process in 200# paint solvent. As Jiang et al. suggested [42], shortening the lithium diffusion path is effective to improve the electrochemical properties. As shown in Fig. 6a, for the pristine LTO materials, the contact area between LTO and LPSCl electrolyte is limited due to the point contacts, resulting in the hindered Li^+ ion transport and high internal resistance. As shown in Fig. 6b, after surface coating of LPSCl on LTO particles, the face-to-face contacts remarkably increase the contact area between LTO and LPSCl and facilitate the lithium ion transport, which enhance the electrochemical performance of the electrodes. What's more, the LTO material and electrolyte particles used in this paper are nanomaterials, so the tiny size of the composite can ensure the large contact area with the LPSCl electrolyte.

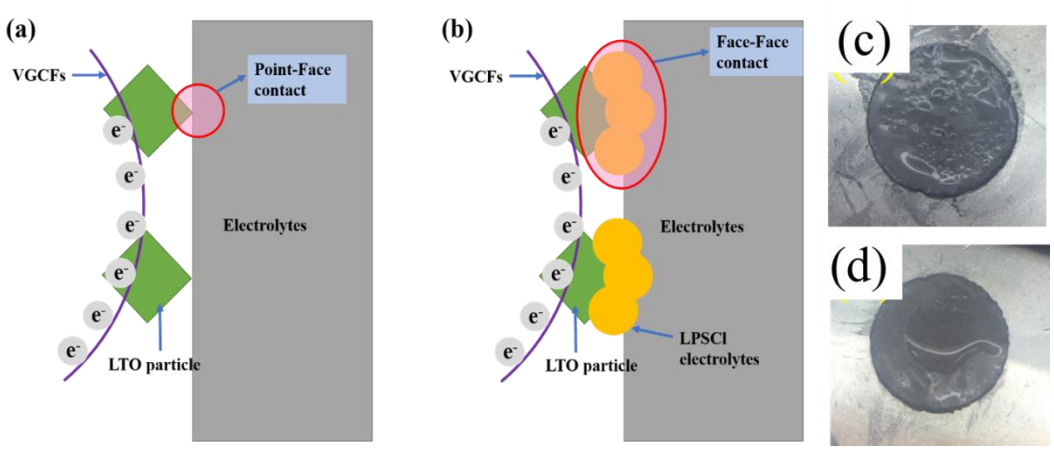

Figure 6. Some possible mechanism to explain the decreasing resistance of the cell with LPSCl@LTO electrode (a) compared with the cell with non-coating electrode (b) and results of wettability of LPSCl in 200#Paint (c) and ethanol (b).

More details about the electrochemical performance of the LPSCl electrolyte with different electrodes are summarized in Table 1. It is indicated that most electrodes matching with the LPSCl electrolyte described in literature have pour utilization of active materials, about 32.6% (LTO-C), 25.0% (S-C), 23.6% (LCO, hand-mixing) and 28.6% (LCO, wet-mixing). Despite 97.8% capacity retention for graphite electrode, the infiltration process is difficult to be carried out in order to achieve a smooth and homogeneous electrode surface. Furthermore, with the update of mixing methods, all-solid-state cells with the LPSCl electrolyte demonstrate better electrochemical performances. This observation agrees with the discussion that further optimization of composite electrode preparation should contribute to a better distribution and so to a higher capacity [39].

Table 1. Electrochemical performance of the LPSCl electrolyte with different electrodes

Electrode	Voltage range/V	Processing method	Electrochemical performance	Ref.
LTO-C	0.5-2.4	Hand-mixing	13 mAh g^{-1} discharged at 50 μA s^{-1}	39
		Ball-milling	57 mAh g^{-1} discharged at 50 μA s^{-1}	
S-C	1.0-3.6	Ball-milling	below 400 mAh g^{-1} after 20 cycles at 0.064 mA cm^{-2}	12
LCO	1.0-2.6	Hand-mixing	33 mAh g^{-1} at 0.1 C after 9 cycles only	40
LCO	2.6-4.2	Wet-mixing	40 mAh g^{-1} during 10 cycles discharged at 0.13 mA cm^{-2}	31
Graphite	0.005-2.0	Infiltration	364 mA h g^{-1} discharged at 0.1 C	41

To further reveal the reasons of the excellent coating performance via liquid-phase post-treatment in 200#Paint solvent, the dispersing property between the solution and LPSCl electrolytes was studied. Ethanol as a comparison sample was investigated, which has been reported as the post-

treatment solvent [43]. It is obvious that the wettability of LPSCl in 200#Paint solvent (Fig. 6c) is superior to that in ethanol (Fig. 6d), which maybe be explained with rules of polarity nearness based on the hydrophobicity of sulfide-based electrolyte and 200# Paint solvent. Consequently, a more uniform dispersion of LPSCl can be formed in the solution during the post-treatment process, leading to uniform distribution on LTO particle surface (Fig. 3c-f) and increased contact area between LTO and LPSCl (Fig. 6b). In addition, the good dispersing of LPSCl also contributes to the distribution of VGCFs, as conductive agent, ensuring the favorable electronic pathways inside electrode. The results indicate that the liquid-phase treatment with 200#Paint solvent is a promising method for forming conformal interface which is beneficial to extensive application of ASSLBs.

4. CONCLUSION

In summary, LTO@LPSCl composite was facilely synthesized via a simple ball-milling and liquid-phase post-treatment with 200#Paint solution, which is firstly applied to ASSLBs to form favourable electrode-electrolyte interface. The LTO@LPSCl/LPSCl/Li cell shows a high capacity of 158.4 mA $h \cdot g^{-1}$ after 250 cycles with excellent capacity retention of about 94.3%. These outstanding properties are mainly attributed to the homogeneously dispersion of LPSCl in the electrodes, which is caused by the good wettability of 200#paint solvent and results in enhanced ion and electronic transport on the interface and low internal resistance between the LTO and LPSCl electrolyte. The simply and effective method in this work provides great convenience and potential for the manufacture and design of others electrode for ASSLBs.

ACKNOWLEDGEMENTS
This work was financially supported by the National Natural Science Foundation of China (Grant No. 21373072 and No.51202047).

References

1. J. M. Tarascon and M. Armand, *Nature*, 414 (2001) 359.
2. J. C. Bachman, S. Muy, A. Grimaud, H. H. Chang, N. Pour, S. F. Lux, O. Paschos, F. Maglia, S. Lupart, P. Lamp, L. Giordano and Y. Shao-Horn, *Chem. Rev*., 116 (2016) 140.
3. K. Takada, *Acta Mater*., 61 (2013) 759.
4. H. Yamada, *J. Indian I Sci*., 96 (2016) 315.
5. R. Kanno and M. Maruyama, *J. Electrochem. Soc*., 148 (2001) A742.
6. A. Hayashi, S. Hama, T. Minami and M. Tatsumisago, *Electrochem. Commun*. 5 (2003) 111.
7. F. Mizuno, A. Hayashi, K. Tadanaga and M. Tatsumisago, *Adv. Mater*., 17 (2005) 918.
8. N. J. J. de Klerk, T. Roslon and M. Wagemaker, *Chem. Mater*., 28 (2016) 7955.
9. H. J. Deiseroth, S. T. Kong, H. Eckert, J. Vannahme, C. Reiner, T. Zaiss and M. Schlosser, *Angew. Chem. Int. Edit.*, 47 (2008) 755.
10. R. P. Rao and S. Adams, *Phys. Status Solidi*. A, 208 (2011) 1804.
11. S. Boulineau, M. Courty, J. M. Tarascon and V. Viallet, *Solid State Ionics*, 221 (2012) 1.
12. C. Yu, L. van Eijck, S. Ganapathy and M. Wagemaker, *Electrochim. Acta*, 215 (2016) 93.
13. K. Takada, N. Ohta, L. Q. Zhang, K. Fukuda, I. Sakaguchi, R. Ma, M. Osada and T. Sasaki, *Solid*

State Ionics, 179 (2008) 1333.
14. K. Takada, *Langmuir*, 29 (2013) 7538.
15. K. Takada, N. Ohta, L. Q. Zhang, X. X. Xu, B. T. Hang, T. Ohnishi, M. Osada and T. Sasaki, *Solid State Ionics*, 225 (2012) 594.
16. N. Ohta, K. Takada, L. Q. Zhang, R. Z. Ma, M. Osada and T. Sasaki, *Adv. Mater*., 18 (2006) 2226.
17. N. Ohta, K. Takada, I. Sakaguchi, L. Q. Zhang, R. Z. Ma, K. Fukuda, M. Osada and T. Sasaki, *Electrochem. Commun*., 9 (2007) 1486.
18. A. Sakuda, H. Kitaura, A. Hayashi, K. Tadanaga and M. Tatsumisago, *J. Electrochem. Soc.*, 156 (2009) A27.
19. J. Haruyama, K. Sodeyama, L. Y. Han, K. Takada and Y. Tateyama, *Chem. Mater*., 26 (2014) 4248.
20. F. Mizuno, A. Hayashi, K. Tadanaga and M. Tatsumisago, *J. Electrochem. Soc*., 152 (2005) A1499.
21. A. Hayashi, Y. Nishio, H. Kitaura and M. Tatsumisago, *Electrochem. Commun*., 10 (2008): 1860.
22. A. Sakuda, H. Kitaura, A. Hayashi, K. Tadanaga and M. Tatsumisago, *Electrochem. Solid St.*, 11 (2008) A1.
23. A. Sakuda, H. Kitaura, A. Hayashi, K. Tadanaga and M. Tatsumisago, *J. Power Sources*, 189 (2009) 527.
24. H. Kitaura, A. Hayashi, K. Tadanaga and M. Tatsumisago, *J. Power Sources*, 189 (2009) 145.
25. S. Teragawa, K. Aso, K. Tadanaga, A. Hayashi and M. Tatsumisago, *Chem. Lett*., 42 (2013) 1435.
26. S. Teragawa, K. Aso, K. Tadanaga, A. Hayashi and M. Tatsumisago, *J. Power Sources*, 248 (2014) 939.
27. S. Teragawa, K. Aso, K. Tadanaga, A. Hayashi and M. Tatsumisago, *J. Mater. Chem*. A, 2 (2014) 5095.
28. F. Mizuno, A. Hayashi, K. Tadanaga and M. Tatsumisago, *J. Power Sources*, 146 (2005) 711.
29. L. Sun, N. Karanjgaokar, K. Sun, I. Chasiotis, W. C. Carter and S. Dillon, *J. Power Sources*, 196 (2011) 6507.
30. T. Ohzuku, A. Ueda and N. Yamamoto, *J. Electrochem. Soc*., 142 (1995) 1431.
31. S. Yubuchi, S. Teragawa, K. Aso, K. Tadanaga, A. Hayashi and M. Tatsumisago, *J. Power Sources*, 293 (2015) 941.
32. P. R. Rayavarapu, N. Sharma, V. K. Peterson and S. Adams, *J. Solid State Electrochem*. 16, (2012) 1807.
33. T. F. Yi, S. Y. Yang and Y. Xie, *J. Mater. Chem*. A, 3 (2015) 5750.
34. X.H. Wu, M. El Kazzi and Claire Villevieille, *J. Electroceram*. (2017), in press.
35. Y. Mo, S. Ping Ong, and G. Ceder, *Chem. Mater*., 24 (2012) 15.
36. H. Kitaura, A. Hayashi, K. Tadanaga and M. Tatsumisago, *J. Mater. Res*., 25 (2010) 1548.
37. Wagemaker, M. Kentgens, A. Mulder and F. *Nature*, 418 (2002) 397.
38. C. Yu, S. Ganapathy, N. J. J. de Klerk, I. Roslon, E. R. H. van Eck, A. P. M. Kentgens, and M. Wagemaker, *J. Am. Chem. Soc*., 138 (2016) 11192.
39. R. P. Rao, N. Sharma, V. K. Peterson and S. Adams, *Solid State Ionics* 230 (2013) 72.
40. J. Auvergniot, A. Cassel, D. Foix, V. Viallet, V. Seznec and R. Dedryvère, *Solid State Ionics*, 300 (2017) 78.
41. D. H. Kim, D. Y. Oh, K. H. Park, Y. E. Choi, Y. J. Nam, H. A. Lee, S. M. Lee and Y. S. Jung, *Nano Lett*., 17 (2017) 3013.
42. C. Jiang, M. Ichihara, I. Honma and H. Zhou, *Electrochim. Acta*, 52 (2007) 6470.
43. F. D. Han, J. Yue, X. L. Fan, T. Gao, C. Luo, Z. H. Ma, L. M. Suo and C. S. Wang, *Nano Lett.*, 16 (2016) 4521.